Free-surface flow of concentrated suspensions

Anugrah Singh [1], Avinoam Nir *, Raphael Semiat

Department of Chemical Engineering, Technion, Haifa 32000, Israel

Received 22 November 2004; received in revised form 6 February 2006

Abstract

Free-surface flows of concentrated suspensions exhibit many interesting phenomena such as particle segregation and surface corrugation. In this work the flow structures associated with free-surface has been studied experimentally. The free-surface velocity for neutrally buoyant suspension of uniform spheres in a gravity driven inclined channel flow was determined by particle imaging velocimetry (PIV) technique. Experiments were carried out for concentrated suspensions with particle fractions ϕ ranging from 0.40 to 0.50. The measured velocities show blunted profile in the channel. The blunting of the velocity profile increases with the particle concentration. The rms velocity fluctuations measured at the free-surface progressively increase with particle fraction ϕ and are linear in shear rate γ. The surface roughness were characterized by analyzing the power spectral density of the refracted light from the free-surface. The characteristics observed are in support of earlier findings.
© 2006 Elsevier Ltd. All rights reserved.

Keywords: Suspension; Free-surface flow; Particle image velocimetry; Shear-induced corrugation

1. Introduction

Free-surface flow of a mixture of solid and liquid with high particle concentration is often encountered in many material processing procedures such as slurry flow in open channels as well as in natural settings such as flood waves carrying extremely high concentration of very fine sediments. The characteristics of such flow are significantly different from those of an equivalent homogeneous liquid. At high particle concentration the hydrodynamic interactions between the particles significantly alter the flow characteristics and we often observe many interesting phenomena, which are not seen in the flow of a Newtonian homogeneous fluid under similar boundary conditions. Shear induced migration of particles is one such phenomenon and this has attracted large number of studies (Leighton and Acrivos, 1987; Phillips et al., 1992; Nott and Brady, 1994; Shauley et al., 1997). Most of the studies on shear-induced particle diffusion are confined to bounded shear flow. Only recently has the free-surface flow of suspension drawn some attention. Tirumkudulu et al.

(2000) in an experiment of partially filled rotating cylinder observed that the migrating particles accumulate in bands along the axis of the cylinder. Timberlake and Morris (2002) studied the phenomena of concentration band dynamics in partially filled annular gap of concentric Couette cylinder with axis of the rotating inner cylinder inclined form horizontal. Subsequent to the experimental investigation of these interesting phenomena there have been a few theoretical analysis to explain the instability mechanism which leads to particle accumulation in bands along the axis of the rotation (Govindarajan et al., 2001; Jin and Acrivos, 2004).

The motivation of the present work comes from another interesting free-surface phenomena observed in flow of concentrated suspensions. In a recent experiment Loimer et al. (2002) have studied the topography of free-surface during the simple shear flow of concentrated suspensions of small inertia-less particles in a viscous fluid. Two parallel belts moving in opposite direction resulted in simple shear flow with the free surface having mean normal along vorticity direction. It was observed that the roughness of the surface disturbances depends on the particle size, particle concentration and on the surface tension of the suspending fluid. It is interesting to note that such phenomena are observed at low flow speeds where Reynolds number is very small. In a model developed to explain this phenomenon they argue that at the free surface the suspension concentration jumps from bulk concentration, ϕ, to zero across a length scale of the order of the particle size. The concentration gradient results into a shear induced particle flux towards the interface, which is balanced by the surface tension restoring force. They have also studied the power spectra of refracted light from the surface in order to study the length and time scale of corrugation structures at the free-surface. Since the relative illumination intensity is associated with the local inclination of the surface, study of temporal and spatial intensity spectra provided valuable information about the wave amplitude and frequency of the surface deformation patterns. It was observed that the disturbances at the free-surface span over wide range of frequency and wavelength. It in interesting to note that the shape of light intensity spectral curves resembled closely that of kinetic energy spectra of turbulent flows. Subsequent to the experiments of Loimer et al. (2002), Timberlake and Morris (2005) have carried out detailed study on the gravity-driven free-surface flow of falling film of neutrally buoyant suspension. They have measured the free-surface velocity profile and film thickness down the channel. Their measurements using the technique of stereoscopic particle velocimetry show particle migration away from the solid surface, which results from gradient in shear rate across the film height. Their model formulation is based on the approach of Morris and Bouley (1999) to calculate the particle flux based on normal stress differences. The free boundary characteristics of the interface is modeled via normal stress jump at the upper surface of the film. The model predictions do show a concentration gradient across the film thickness, which is in qualitative agreement with the experimental results, but overestimates the concentration at the free-surface. Timberlake and Morris suggested that this could be due to an improper boundary condition at the free-surface. This adds to the importance of understanding the correlation between the surface topography and flow structures at the free interface. However, qualitative agreement of their model which is based on the normal stress differences do suggest their role in explaining free-surface instabilities. Brady and Carpen (2002) argue that there is an instability mechanism in non-Newtonian fluids when a jump in normal stress is present between the two fluids. Using stability analysis they have shown that the flow of fluids with a negative second normal stress difference can become unstable with respect to transverse and span wise perturbations. Using their analysis they have illustrated the instability mechanism for two-layer Couette and falling film flows of viscous suspensions. Their theory finds considerable support from the simulation and experimental studies on normal stress measurements for non-Brownian suspensions at low particle Reynolds number. In viscous suspensions we observe large second normal stress difference (Zarraga et al., 2000; Singh and Nott, 2003) which leads to instability at the interface as shown in the analysis of Brady and Carpen (2002).

Study of flow structure at the free-surface in the turbulent regime has attracted many experimental studies. Rashidi et al. (1992) have studied the wave-turbulence interaction in free-surface channel flows. This was achieved through flow visualization using very small oxygen bubbles as tracers. A high-speed camera could record the flow structure and free surface movement. Kumar et al. (1998) studied the flow structure and characteristics of free-surface turbulence in channel flow. They measured the stream wise and span wise velocities at the free-surface by PIV. The surface normal velocities were then estimated by continuity.

Despite numerous studies on free-surface flow of pure fluids there are no reported experiments on the characterization of surface deformation and the interface velocities for free-surface flow of concentrated suspensions in creeping flow regime. Such flows are different from pure fluid flow in many ways. Although the

suspending fluid is incompressible, the compressibility of the particle phase can cause them to reorganize and form structures. The purpose of the present work is to investigate further the work of Loimer et al. (2002) and study the characteristics of free-surface motion and corrugation structure at the free-surface in shear flow of concentrated suspension. Our objective is also to study the effect of concentration on the velocity and the amplitude of fluctuations near the free-surface which is required to characterize the particle size scale flow structures in free-surface flow of suspensions. Moreover the fluid flow measurement at the free interface is of fundamental importance to application to material processing as the surface effect is particularly manifest at the interface where the transport of mass, momentum and energy are affected.

We have used PIV technique to perform the measurement of velocities near the free-surface. Power spectral densities (PSDs) were computed from the intensities of the refracted light from the free surface. These PSDs are used to characterize the surface roughness of the flowing suspension. Section 2 describes the experimental facilities and procedures including the optical arrangements and PIV analysis method. The materials used and method of preparation is explained in Section 3. Section 4 will present the results from our measurement followed by conclusion in Section 5.

2. Experimental facilities and procedures

2.1. Channel and flow apparatus

Fig. 1 shows the schematic diagram of our experimental setup. The experiments were conducted in a rectangular channel made of Plexiglas. The channel was 40 cm long, 2 cm wide and 5 cm deep. In the figure, x is the spanwise direction, y is the flow direction and $-z$ is the gravitational direction. The two ends of the channel were connected via circular tubes of diameter 2 cm to a screw pump, which recirculated the suspension in the channel. The screw pump was specifically designed to handle suspension of large particles. The clearance
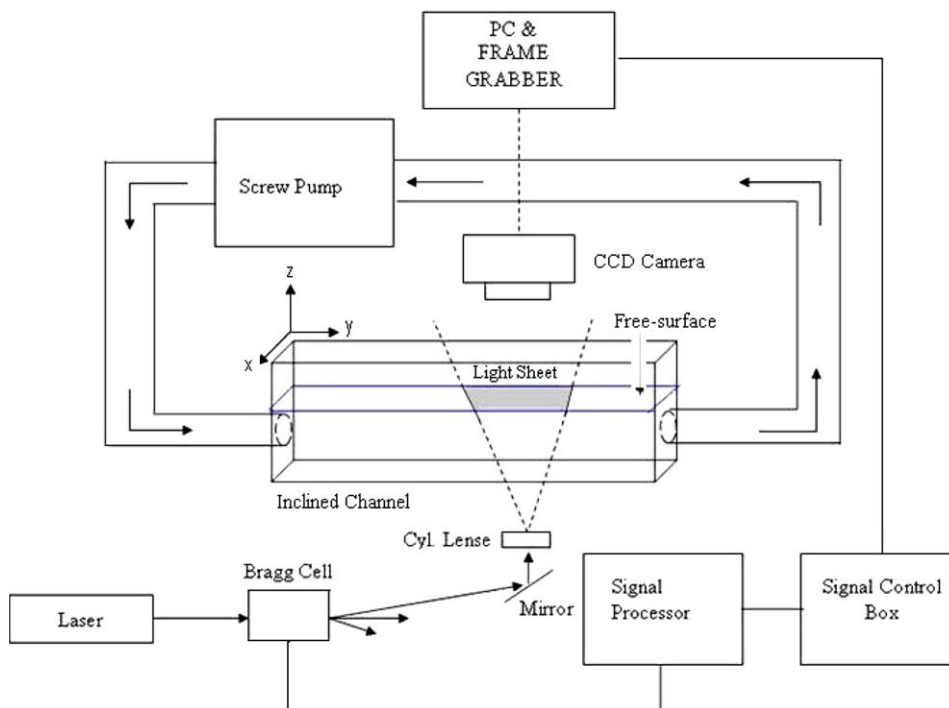

Fig. 1. Schematic diagram of the flow geometry and optical arrangements. The channel is slightly inclined to the horizontal to enable gravity driven flow of suspension.

between the screw and barrel of the pump was 5 mm. The speed of the screw pump and the inclination of the channel could be adjusted to get the desired flow. The suspension in the channel was filled to a level such that the free-surface in the x–y plane was always above the inlet and outlet regions. The optical arrangements (described in the next section) imaged the free-surface in the middle portion of the channel. The maximum (centerline) velocity in the channel used in our study varied from 1 to 4 cm/s. The maximum shear rate γ reached in our experiments was less than $10 \, s^{-1}$. Thus, for particles with a typical radius, a, of $O(10^2 \, \mu m)$ and a fluid with kinematic viscosity, v, of $O(1 \, cm^2 \, s^{-1})$, the Reynolds number based on particle size (as given below) was negligibly small

$$Re_p = \frac{\gamma a^2}{v} < 10^{-3} \tag{1}$$

and, yet, smaller if the effective viscosity of the suspension is considered.

2.2. Optics for PIV images

Particle image velocimetry (PIV) is a non-intrusive, full field optical measuring technique. PIV is used to obtain velocity information about fluid motion and has been applied to a many kinds of flows. In traditional PIV experiments, the fluid of interest is seeded with tracer particles, which are illuminated by a sheet of bright light. The positions of these particles at different times are recorded on a camera and the image sequence is digitized. Particle distance between two successive images ascertains the motion of the fluid. In multi-frame/single exposure PIV, two images revealing the positions of tracer particles within the fluid are taken at short time, Δt, apart (Adrian et al., 1995). Since it is not possible to track individual particles, so a statistical analysis is required. Each image is divided into a grid of small sections called as interrogation areas. The corresponding interrogation areas within each of the two images are then cross-correlated. The cross-correlation function is effectively a pattern matching routine that determines which displacement is required to shift the first area to best overlap the second area. By scaling this area by the magnification of the camera lens and dividing by Δt, the average velocity for the fluid within the interrogation area is obtained. This process is repeated at each grid point within the image, resulting in a map of velocity vectors to describe the flow.

The optical system is sketched in Fig. 1. An Argon ion continuous laser (actual power 0.16 W) was used as light source. In order to get two pulses at short time interval a Bragg cell was placed ahead the laser beam. This optical device splits the continuous beam into main beam (continuous) and several lateral beams whose frequency can be adjusted by a signal control device. A mirror reflected one of the lateral beams (usually the first one), which was then used to generate a horizontal light sheet (shown by the shaded region in the x–y plane of the Fig. 1) using a cylindrical lens.

The images were captured using a 1360×1024 pixel CCD camera (PixFly from PCO) in conjugation with a lens of 100 mm focal length. The camera can either operate in fixed mode (Video mode) to capture images at 19 frames per second or in Double Shutter mode. In Double Shutter mode, two separated image frames with a short interframing time can be captured. An in-house-fabricated TTL electronic circuitry generated two short pulses, which were fed to the signal processor connected to the Bragg cell. The camera was triggered externally which synchronized with the two pulses. With this arrangement it was possible to acquire images with interframing time between 1 μs and 20 ms.

The free-surface was visualized by seeding the flow with hollow glass particles of diameter 5–10 μm. Fig. 2 shows a representative PIV photograph of the free-surface in x–y plane. With the lens operating at magnification of 0.7 the view of the flow field (9.1×6.8 mm) was captured. The size of the tracer particle images varied between 2 and 4 pixels.

2.3. Interrogation of PIV photographs

The digitized photographs were saved in 680×512 pixels, 12 bits format gray scale images on a computer via frame grabber. The image scaling was determined by taking the photograph of a grating, which had 1000 lines/inch.
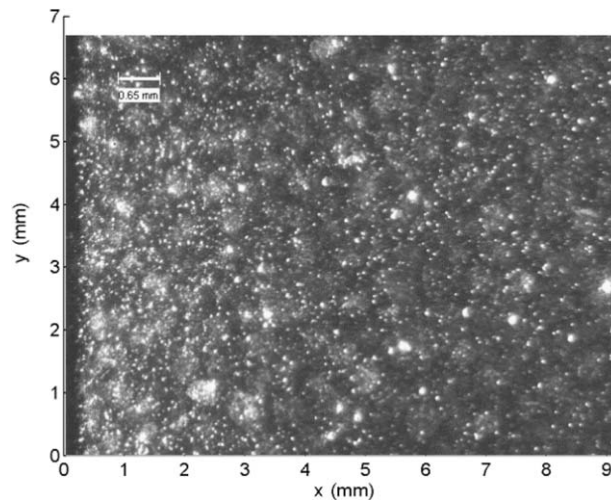
Fig. 2. A sample PIV image of tracer particles at the free-surface of the channel.

To calculate the free-surface velocity from pair of images we have used the PIV analysis software PIV SLEUTH (Christensen et al., 2000). The image pairs were interrogated using two-frame cross-correlation technique of Adrian et al. (1995). Two-frame cross-correlation is a highly accurate method. In this method the pair of images are imaged onto separate frames. Such correlation gives only a single displacement peak and hence is ideal for flows that have flow reversal. Unlike auto-correlation or one-frame cross-correlation it does not require information about the mean flow direction. In our experiments the time difference between two images was 52 ms when images were recorded with camera working in fixed mode of 19 frames/s. For larger velocities we operated the camera in double shutter mode where the inter-framing time was between 5 ms and 20 ms. The spot size for flow field interrogation was 64×64 pixels with 75% overlap between interrogation spots. Thus the size of the interrogation window was approximately 0.91 mm $\times$ 0.91 mm and the distance between two adjacent interrogation windows was about 230 μm. The size of interrogation window was found to be the minimum size for accurate processing at the current concentration of the seeded particles. This size was estimated by processing the images with interrogation window sizes varying from 32×32 pixels to 128×128 pixels and choosing the size that resulted minimum spurious vectors. This interrogation resulted in, approximately, 27 rows and 38 columns of vectors for each image. The good quality images insured that very few wrong vectors were computed. Vectors with low signal to noise ratio were removed and replaced with the interpolated vectors from nearest points.

3. Preparation of suspension

To get good quality images of the seeded tracer particles it is required that the refractive index of suspending fluid and suspended particles are closely matched. The refractive index matched suspension removes unwanted scattering from the suspended particles. Preparation of neutrally buoyant suspension required additional criterion of density matching of fluid and particles. In our study the particles used in preparing the suspensions were PMMA spheres of mean diameter 655 μm and 150 μm. The suspending fluid chosen was Newtonian organic liquid (TR 11510) obtained from Cargille Laboratories (Cedar Grove, NJ). This liquid was chosen as its density 1.18 g cm^3, and refractive index 1.491 closely matched those of the PMMA particles. The liquid had a viscosity of approximately 2 Poise and a surface tension 46 dyne/cm. Approximately 800 ml of suspension were needed to fill the flow apparatus. To prepare the suspension requisite amount of particles and liquid were added in a beaker and stirred vigorously to achieve homogeneous mixing and dispersion of the particles. However, during the mixing small air bubbles were formed which needed to be removed. This was achieved by keeping the suspension under vacuum for 2–3 days, allowing the bubbles to rise up. Suspension cleared of air bubbles was transferred into the channel very slowly.

4. Results

4.1. Velocity measurements

We have measured the velocity at the free-surface across one half of the channel. The velocity measurements were carried out at a distance 20 cm down the channel. At this distance the macroscopic profile was nearly fully developed beyond entrance effects, while no significant deviation from a homogeneous particle distribution due to shear-induced migration should be expected. We would like to mention that the images taken were only up to 9.1 mm from the channel wall, little less than half width (10 mm) of the channel. The length of image in flow direction was 6.8 mm. To get the mean velocity profiles, an average of 150 velocity vectors was taken which were obtained by cross-correlation analysis of 150 consecutive pairs of images. Figs. 3 and 4 show the mean velocity (in flow direction) plotted against distance from the wall, i.e. from 0.5 mm (first interrogation window) to about 8.5 mm (last interrogation window). The mean velocities are scaled with the maximum velocity V_m in the channel. Fig. 3(a) shows the y-velocity profile at various V_m for suspension with particle concentration of 0.45. The figure illustrates that increasing the mean velocity does not change the profile significantly. This indicates that our measurements were carried out for fully developed flow. Moreover,
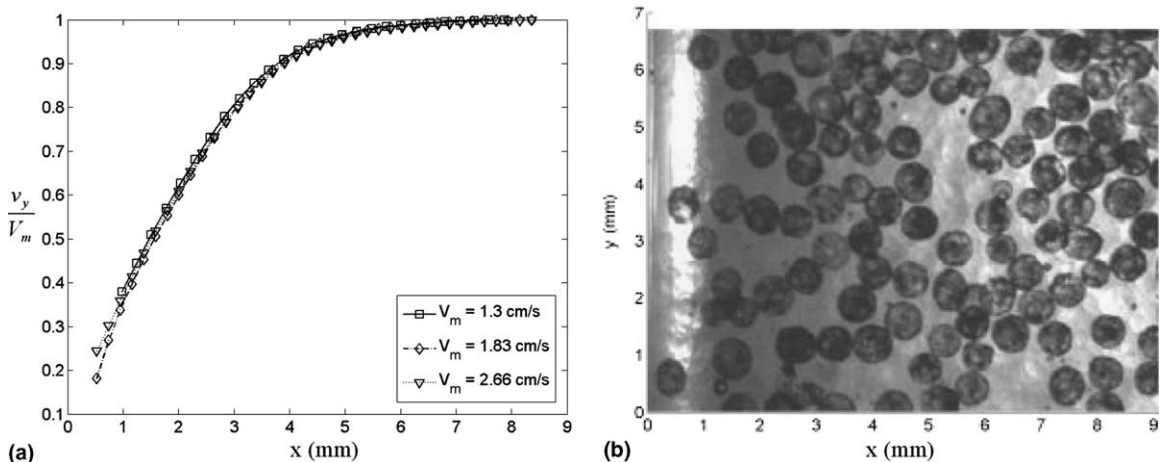

Fig. 3. (a) Mean y-velocity profile across the channel at various centerline velocities for suspension of 45% concentration and particle size 650 μm. (b) Visualization of concentration profile at the free surface showing uniform concentration across the channel.
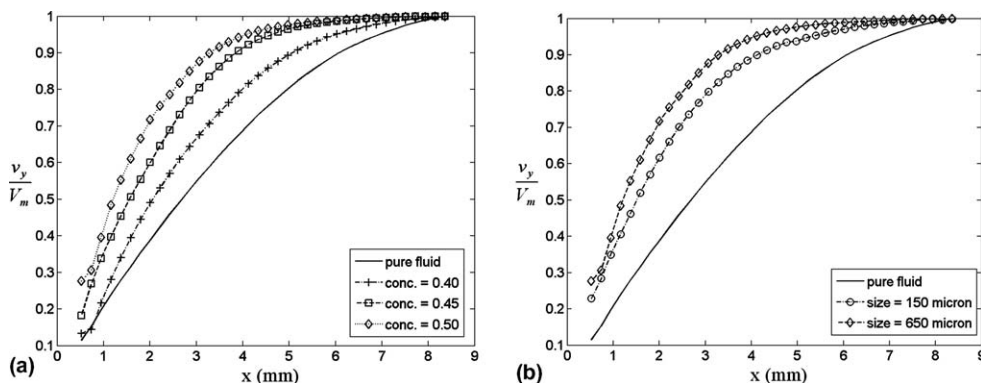

Fig. 4. (a) Mean y-velocity across the channel at different concentration of suspension with 650 μm particles. (b) Mean y-velocity across the channel at two different particle sizes. The particle concentration was 45% in this case.

the mixing in the screw pump and the small length of channel insured that lateral particle migration across the channel remained minimal. To verify this we conducted one experiment in which a small fraction of the suspending particles were dyed in black color. The image of these particles (see Fig. 3b) shows uniform concentration across the channel width except a small region close to the wall. This indicates that there is no appreciable migration in the x–y plane for which we report the velocity profiles. Fig. 4(a) shows the effect of particle concentration on the velocity profile. The deviation from the parabolic profile (corresponding to the pure suspending fluid) becomes pronounced as the particle fraction increases from 0.40 to 0.50. The profile can be roughly divided into a shear region nearer to the wall and a plug flow region near the center of the channel. As the concentration increases the span of the plug flow region also increases. The blunting of velocity profile in absence of appreciable particle migration is interesting as many authors (Leighton and Acrivos, 1987; Phillips et al., 1992) have related this to particle migration. Karnis et al. (1966) and Sinton and Chow (1991) on the other hand report velocity blunting but no measurable non-uniformity of particle concentration. Koh et al. (1994) have measured the velocity and concentration profile in pressure driven flow of concentrated suspension in a rectangular channel. Based on their measurements they speculate that there could be a significant 'slip' between the particles and the suspending fluid which increases with increasing particle concentration and size. Our measurements of the fluid velocity near the wall do indicate a slip velocity which increases with the bulk particle concentration. The observed blunting of velocity profiles in absence of migration may be attributed to this phenomena.

Timberlake and Morris (2005) have measured the free-surface velocity profile at various axial positions down the inclined channel for film flow of suspension. The differences between the macroscopic velocity profiles in this work and that by Timberlake and Morris (2005) that result from the difference in the experimental setup, as channel dimension and film depth, and from the intensity of the shear-induced particle migration that prevailed in the latter work. Their results taken at the axial location where the flow is fully developed show that the free-surface velocity profiles do not depend upon the film thickness and the angle of inclination of the channel. Their measurements show that in fully developed flow the scaled velocity profiles are the same for particle fraction $\phi = 0.30$ and 0.40. This can be attributed to the shear-induced migration of particles from the bottom solid surface toward the top free interface and their accumulation there (Leighton and Acrivos, 1987). From the similarity of the gravity-driven free-surface flow of falling film of a suspension and the pressure driven close duct flow it is expected that the particle concentration at the free-surface will reach a constant (maximum) value. This process appears to have been significant in their study as the film thickness was small, varying from 1.8 to 4 mm. Our results in Fig. 3(a) are in support of this observation. However, our plot of free-surface velocity profiles at various particle concentrations (Fig. 4a) shows a behavior different from the observation of Timberlake and Morris. Our experiments for open channel flow are different in that there is no significant migration due to the relatively short length of the channel and the fact that the depth of the suspension in our study was relatively large, about 2 cm. It is expected that our measured free-surface velocity will depend on the surface particle concentration which, in our study, is same as that in the bulk and is kept uniform by the continuous mixing of the suspension in the screw pump. It is interesting to note that the model predictions of Timberlake and Morris for the velocity profile indicates that the scaled velocity will become more flat with increase in particle concentration, ϕ, as observed in our studies.

In Fig. 4(b) we have plotted the scaled velocity profiles for suspensions with two different sizes of particles. We observe that for suspension with larger particles (650 μm) the profile becomes more flat compared to that with smaller particles (150 μm), indicating that the slight particle migration that does exist in the system is more pronounced with the bigger particles.

Next we consider the profiles of velocity fluctuations across the channel. The time averaged velocity fluctuations, u', were computed in the following manner:

$$u' = \sqrt{\overline{(u - \bar{u})^2}}, \tag{2}$$

where u is the instantaneous velocity, $\bar{u}$, the local mean velocity and overbar denotes the time average. One hundred and fifty velocity vectors were considered for taking the time averaged root mean squared (rms) velocity fluctuations. Fig. 5 shows the root mean squared x and y velocity fluctuations across the channel. As expected both x and y velocity fluctuations are maximum near the wall of the channel where the shear rate
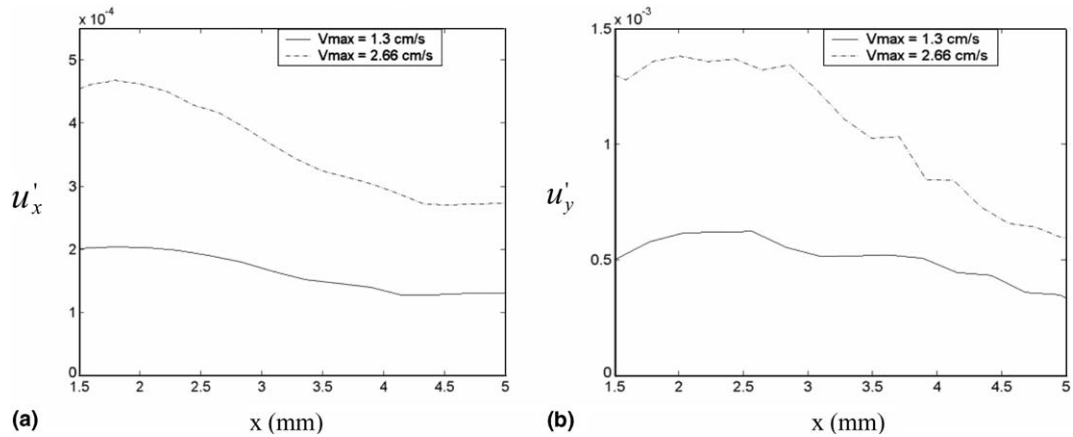
Fig. 5. Root mean square (rms) of x-velocity fluctuations (a) and y-velocity fluctuations (b) at two different centerline velocities. The concentration of 650 μm sized particles was 45%.

is maximum and they fall away from the wall. The fluctuations increase with increase in the centerline velocity. In Fig. 6(a) and (b) we have scaled the x and y component of velocity fluctuation by the local shear rate and plotted against the axial position. Both x and y velocity fluctuations follow linear relationship with shear rate in the region of appreciable velocity gradients near the side wall. It is argued that in Stokesian suspensions the particle stresses and the fluctuating motion arises from the many body interactions even if there are no non-hydrodynamic forces (Jenkins and McTigue, 1990; Nott and Brady, 1994; Singh and Nott, 2000). Zarraga et al. (2000) and Singh and Nott (2003) have experimentally measured the particle stresses, which are linear in shear rate. Koh et al. (1994) have reported the standard deviation of the velocity in addition to the average velocity profile in the pressure driven flow of suspension in closed rectangular channel. The magnitude of standard deviation decreases from the wall to the center of the channel. Our results support their observation and provide experimental measurement of velocity fluctuations in suspension which are linear with shear rate. We also observe that as the particle fraction increases the velocity fluctuations also increase. We also observe increase in the velocity fluctuations away from the wall where the shear rate is much smaller. In the absence of any significant velocity gradient, the presence of velocity fluctuations may be attributed primarily due to conduction of fluctuations by particle–particle interactions. It is important to note that we have based our interpretation on velocity fluctuations in shear zone. Away from the wall in the plug flow region, the shear
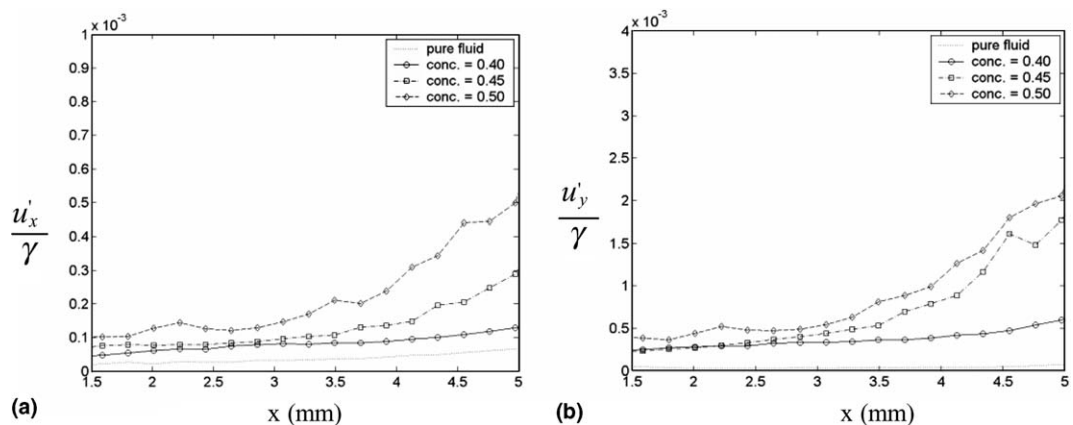

Fig. 6. Root mean square x-velocity fluctuation (a) and y-velocity fluctuations (b) scaled with local shear rate. The particle size and concentration being 650 μm and 45% respectively.

rate becomes very small and the mean velocity is large. This makes the findings of auto-correlation peaks in the interrogation windows less reliable.

4.2. Flow structures and free-surface deformations

The surface images were taken by placing the camera above the surface and illuminating the channel from below using a cold light source. The light source was placed at an appropriate angle so that it reached the camera lens after refraction from the free-surface. The corrugated surface refracted the light depending upon the local free-surface orientation. Fig. 7(a) shows a typical image of the deformed free surface for suspension with 40% particle fraction. Fig. 7(b) shows magnified image of the surface illuminated by a light source kept above the free-surface. The surface roughness patterns are similar to those observed by Loimer et al. (2002). The wide spectrum of surface curvatures is clearly visible in Fig. 7(b).

To visualize the structures at the free-surface we sprinkled very small quantity of hollow glass spheres of 5–10 μm diameter. The camera placed above the free-surface took snapshots at 19 frames/s. The laser light sheet illuminated the surface from the side and the glass spheres produced shining structures. Very low concentration of these tracer particles on the surface insured that there was no effect on surface tension (Kumar et al., 1998). In the Fig. 8(a)–(d) we observe flattering motion of vortical structures in four consecutive frames. These structures, which are result of vortical motion produced by the rotating particles, are observed close to wall where shear rate is appreciable.

To obtain the velocity field associated with these vortical structures we have used particle image velocimetry (PIV) technique. The flow was seeded with small glass particles of 5–10 μm diameter (used as tracers) and not sprinkled on the surface. The free-surface was illuminated by laser light sheet and images were captured by the CCD camera. The image frames were then analyzed using the PIVSLEUTH software to obtain the velocity fields. Fig. 9(a) shows the instantaneous velocity vectors for suspension of 40% particle fraction. The maximum centerline velocity was 2 cm/s. In Fig. 9(b) we have computed fluctuation fields by subtracting the mean velocities from the instantaneous velocity field. Since the flow field is present with wide range of velocities, it was difficult to choose the correct time interval between two sets of frames, which would resolve the whole flow field. In most of our studies we chose the interframing time small enough to resolve the fluctuation fields in the region of appreciable shear gradient but large enough to resolve the vectors in the plug flow region.

The flow structures are distinct in the region close to the wall. In order to see the vortical motion associated with the particles, we have computed the vectors in the region away from the wall where the flow field is characterized by narrow range of velocities. It was possible to choose the interframing time, which clearly resolved the flow field. Fig. 10(a)–(d) shows the motion of vortical structures with four consecutive frames. The interframing time was 52 ms when the camera operated in fixed frame mode. The vortical structures, which are
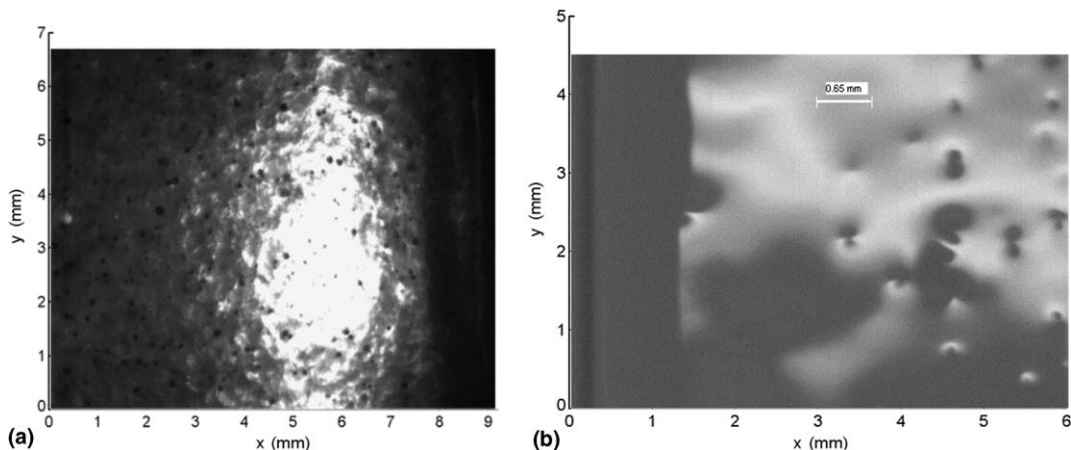

Fig. 7. Free-surface roughness patterns for suspension with particle fraction 40%. The inset in the photograph shows the particle size scale (650 μm).
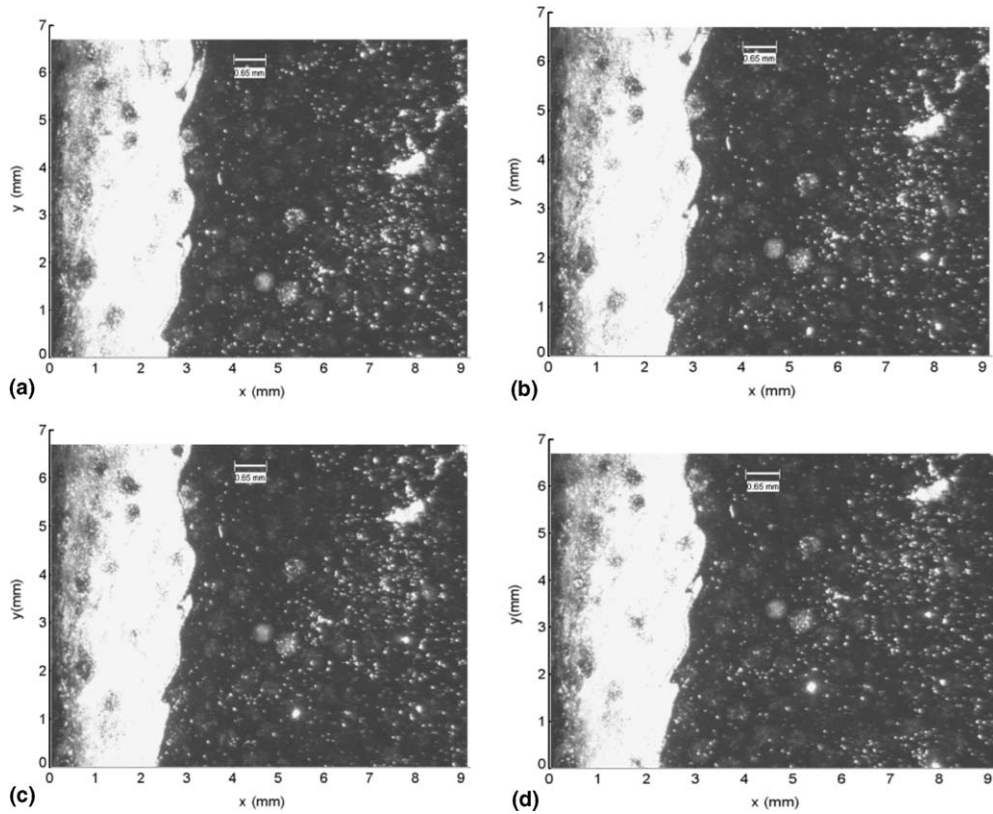
Fig. 8. Visualization of flow structures using tracers sprinkled on the surface. Images (a)–(d) are four consecutive frames with inter-framing time of 52 ms. The particle fraction for this experiment was 45% with centerline velocity being 1.6 cm/s. The particle size scale (∼650 μm) is also shown in the photographs.
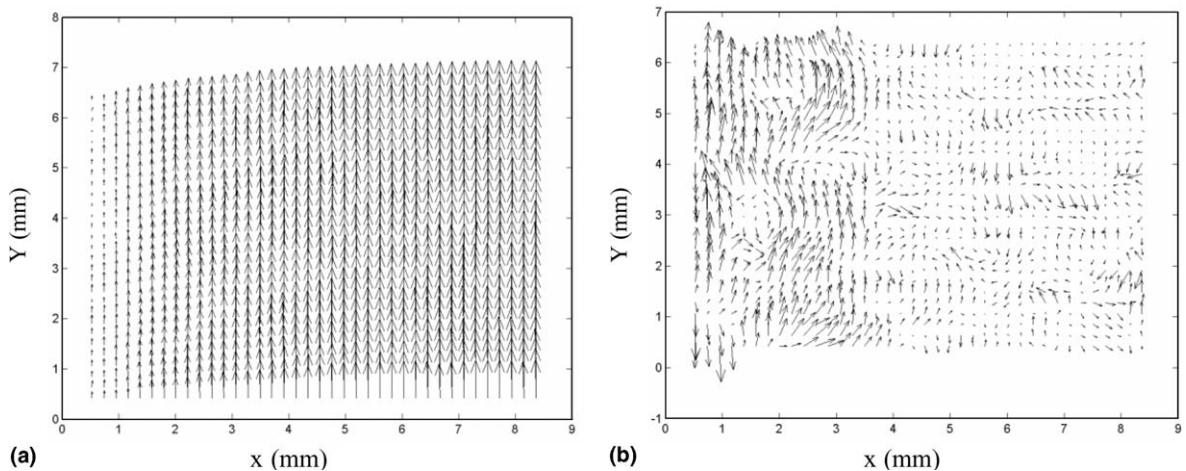

Fig. 9. Vector map of velocity field (a) and fluctuation velocity field (b). The particle fraction for suspension of 650 μm particles was 40% and the maximum centerline velocity was 2 cm/s.

advected with the mean flow field, can be seen in these frames. Though the smallest length scale is particle size, we observe these structures, which are much larger, compared to the particle diameter. The regular pattern of these vortices distinguishes it from a fully developed turbulent structure. However, in fluid mechanics it is well
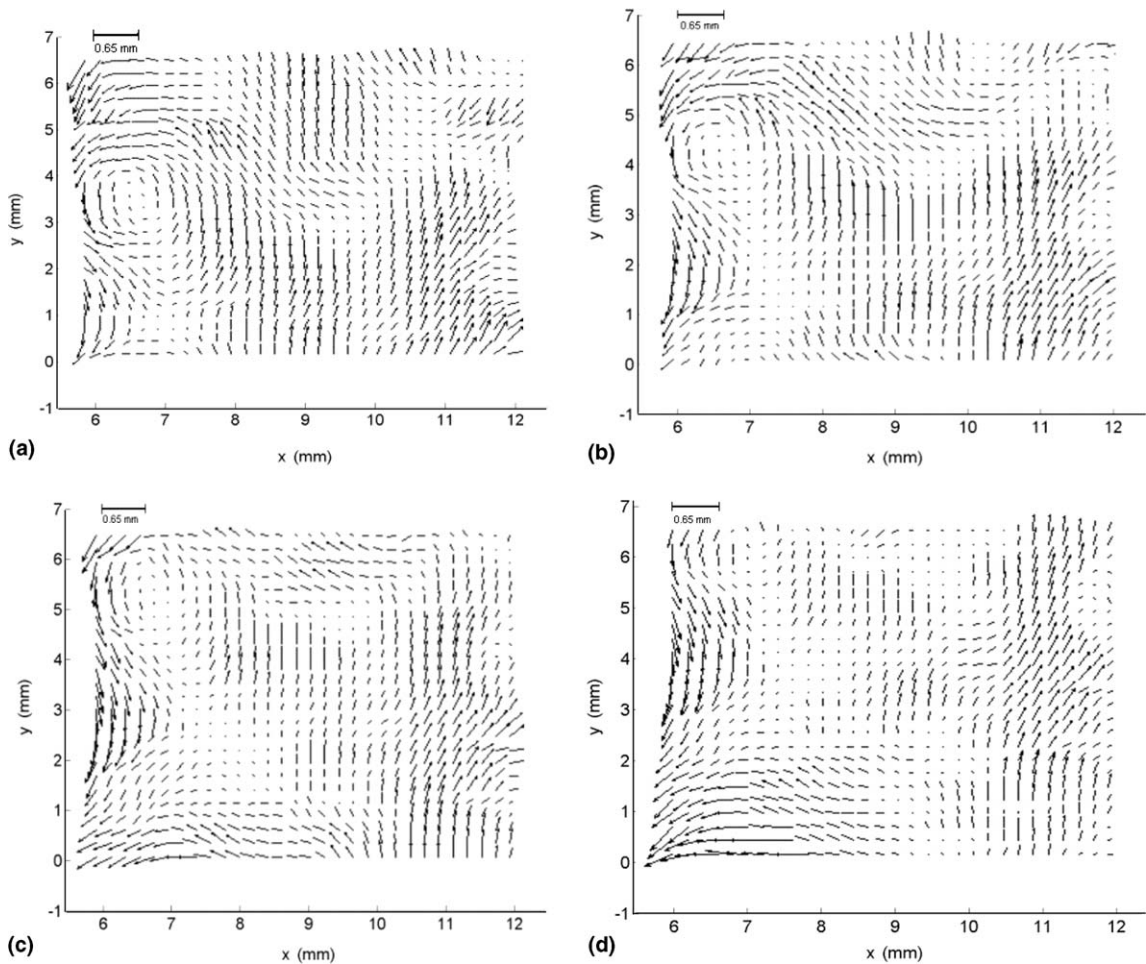
Fig. 10. Vector plot of fluctuation velocities at 40% concentration of particles. The centerline velocity for this case was 1.65 cm/s. The particle size scale (∼650 μm) is also shown in the images.

known that flow instabilities lead to the formation of patterns which strongly affect the dynamics, yielding coherent structures and controlling the transition to turbulence.

The instantaneous fluctuation velocity field in Fig. 11(a) and (b) shows that as the particle concentration increases the region of these flow structures becomes confined very close to the wall. This observation is also supported by the finding that with increase in particle concentration the flow direction velocity profile becomes more blunt, i.e. the plug flow region of the profile shifts close to the wall.

4.3. Spectral analysis

We present here the power spectral densities of image intensity for both temporal and spatial directions. Though the exact relation between the surface curvature and intensity of the image is not known, such spectra do provide a qualitative estimate of the length and time scale of the surface roughness. Such analysis along with the PIV data can increase the understanding of the free-surface flow, its scales and the nature of the flow structures. The near surface particle fluctuation causes deformation of the interface. When the deformation relaxes, the energy contained within it is released back into the fluid. This may further affect the surface topography elsewhere. In the turbulence literature this energy cascade is revealed by the turbulent kinetic energy spectra. However the correct analysis of the kinetic energy spectra requires continuous velocity measurements at small time intervals. Since this was not possible from our velocity measurements we have studied the spectra
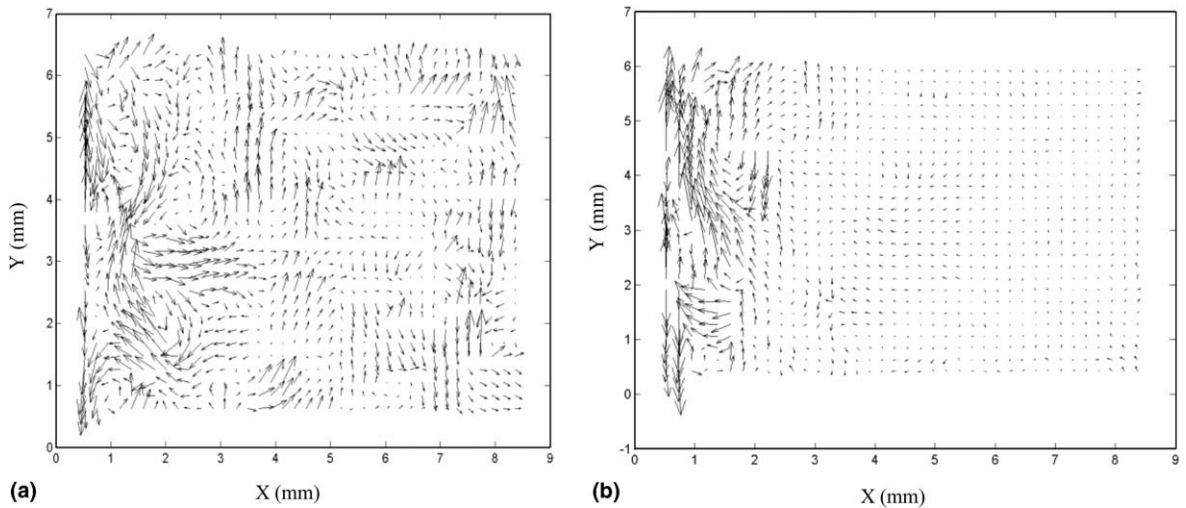
Fig. 11. Vectors of fluctuation velocities at 45% (a) and 50% particle concentration (b). The centerline velocities were 2.65 and 1.19 cm/s respectively. The particle size was 650 μm.

of the image intensity. For temporal measurements photographs were taken at a frame rate of 19 frames/s. Since the shear rate across the channel was not constant, we computed the power spectral density at fixed lateral location. Around this point within an area of 10×10 pixels a power spectral density (PSD) was computed using fast Fourier transform. 100 PSDs were averaged to obtain the PSD distribution such as in Fig. 12(a) and (b). A total of 1024 frames were taken to get the PSDs except for suspension with particle concentration of 0.40 for which only 256 frames were taken. These plots show large peaks at regular intervals indicating the presence of flow structures at multiples time scale. The length scale associated with the flow structures can be estimated by using the Taylor hypothesis i.e. multiplying the time scale with the local average velocity at that position. The smallest length scale is of the particle size which corresponds to wave number of ~ 1.5 mm^{-1} for 655 μm sized particles.

For spatial PSDs measurements in flow direction (y) an area of full image height, 512 pixels and a width of 10 pixels around a point of interest was taken. The PSDs were averaged for 25 uncorrelated frames. Similarly for PSDs perpendicular to the flow direction (x-direction) the area of full image width, 680 pixels and a height of 100 pixels were taken and averaged over 25 uncorrelated frames. From the same data the auto-correlation
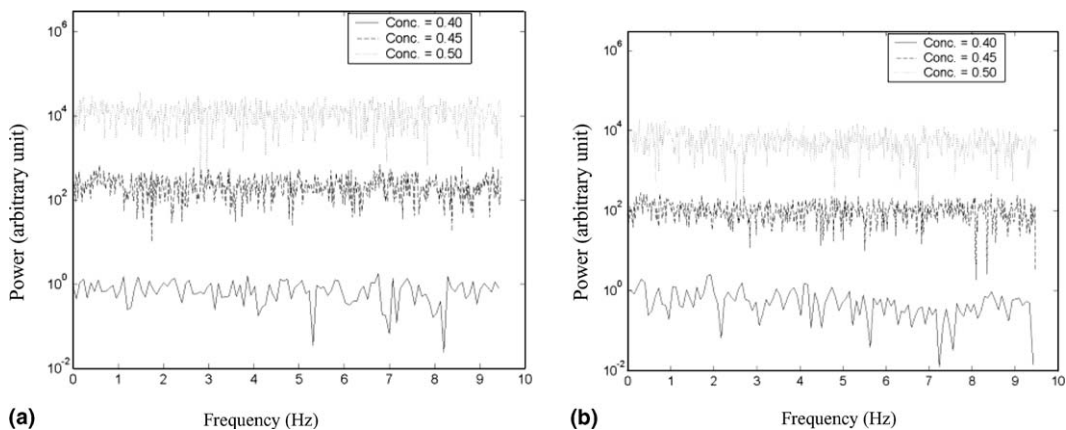

Fig. 12. Temporal PSD for 40%, 45% and 50% particle concentration. (a) At locations corresponding to shear rate $= 2$ s^{-1}. (b) Near the wall. For clarity the normalized PSDs have been multiplied by factors of 1, 10 and 100 for particle fractions 0.40, 0.45 and 0.50, respectively. The particle size was 650 μm.
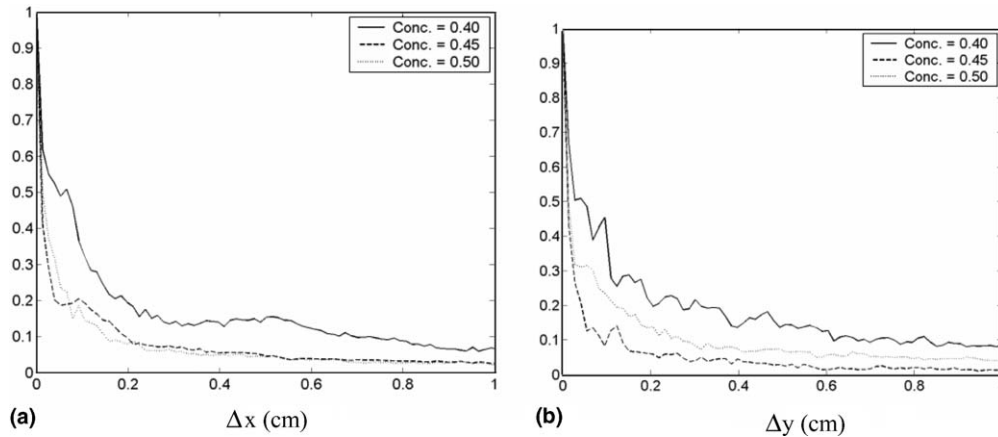
Fig. 13. Normalized spatial auto-correlation in x-direction (a) and y-direction (b) at shear rate 2 s^{-1}.

functions were computed. These correlation functions represent how the flow structure at a location is correlated with that at some downstream location. In Fig. 13 we present spatial auto-correlation in x- and y-directions for suspensions with particle fractions 0.40, 0.45 and 0.50. Since the experiments at different particle concentrations were not carried out at the same centerline velocities it is difficult to make a comparison from the spatial correlation in x-direction as shown in Fig. 13(a). The spatial auto-correlation in flow directions was evaluated at positions where shear rate was 2 s^{-1}. The plots for different concentrations reveal that the flow structures uncorrelated faster for particle concentration of 0.45 compared to the particle concentration of 0.40. However with particle concentration of 0.50 we observe that the auto-correlation decays slower. This observation is in agreement with the earlier findings of Loimer et al. (2002) who report maximum disorder at particle concentrations between 0.40 and 0.45. The rate of decay of auto-correlation is related to the flow structures. At low concentration the particle fluctuations are not strong enough and the flow structures convect with the mean flow. On the other extreme i.e. when the particle fraction approaches to maximum packing fraction, the particles again follow ordered motion due to crowding effect. There exists a critical particle fraction value when the fluctuations are strong enough to produce wide spectrum of uncorrelated flow structures.

In Fig. 14 we show the effect of shear rate on the decay of spatial auto-correlation in flow direction. Auto-correlation functions were computed at different lateral locations corresponding to shear rates of 2, 5, 6 and
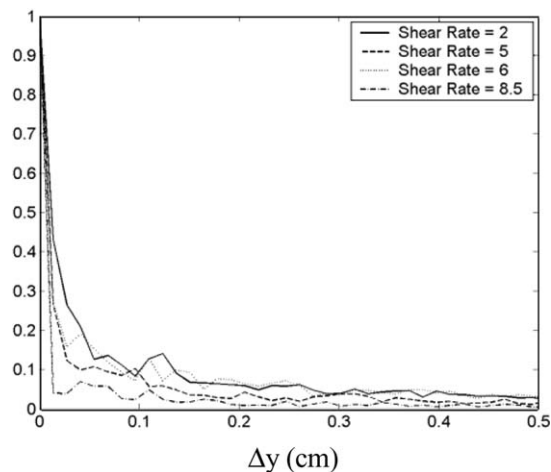

Fig. 14. Normalized spatial auto-correlation in y-direction at different shear rates. The concentration was 45% for the suspension of 650 μm particles.

$8.5 \ s^{-1}$. The particle concentration was constant at 45%. As the shear rate increases the rate of decay of auto-correlation functions also increases i.e. the flow structures become more un-correlated. At the location of low shear rates the disturbances are mostly advected with the flow while that at high shear rates it is soon destroyed and new disturbances are created.

Spatial PSDs are very useful in length scale estimation of flow structures. In Fig. 15(a) and (b) we present spatial PSDs in x- and y-directions, respectively for suspensions with particle fractions of 0.40, 0.45 and 0.50. The spectral densities in the span-wise direction (Fig. 15a) do not show any concentration dependence. The spectra in x-direction (span-wise direction) did not show any systematic variation to make any conclusive observation. In Fig. 15(b) the PSDs in the flow direction were evaluated at positions corresponding to shear rate of $2 \ s^{-1}$. For clarity, we have multiplied the normalized PSDs with factor of 1, 10 and 100 for particle concentrations 0.40, 0.45 and 0.50 respectively. It can be observed that the relative decay to high wave number content is more pronounced for the suspension with higher concentrations. It suggests that the distribution of power along the cascade of wave number is influenced by the concentration of particles and the dissipation of
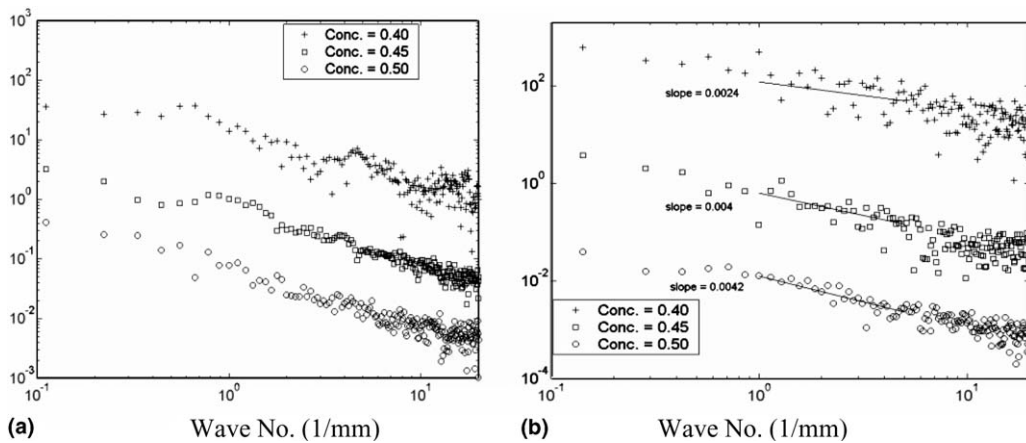

Fig. 15. (a) Normalized spatial PSDs in x-direction and (b) normalized PSDs in y-direction. The PSDs were evaluated at positions where shear rate was $2 \ s^{-1}$.
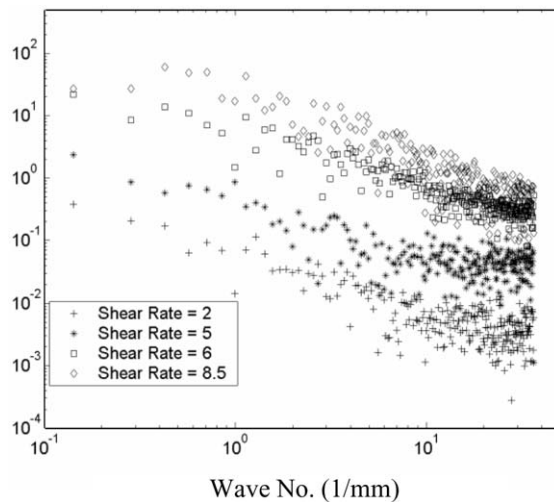

Fig. 16. Normalized spatial PSDs in flow direction at different shear rates. The particle concentration was fixed at 45% for the suspension of 650 μm particles.

power is enhanced towards low wavelength region at higher concentrations. These results are similar to the observation of Loimer et al. (2002) and Timberlake and Morris (2005).

In Fig. 16 we have evaluated PSDs in flow direction corresponding to different lateral positions at which the shear rates were 2, 5, 6 and 8.5 s^{-1}, respectively. The particle concentration was fixed at 45%. The relative similarity of curves indicates that there does not seem to be influence of shear rate, a result also supported by the findings of Loimer et al. (2002). Timberlake and Morris (2005) have also observed that the experiments run under constant particle fraction and inclination angle at varying film thickness (and hence varying shear rates) have PSDs of very similar wave number content. This suggests that in our experiments the surface topography is isotropic but is influenced by the particle concentration.

5. Conclusion

We have studied the free-surface flow of concentrated suspension in channel flow with the tool of particle image velocimetry. It was observed that as the concentration increases the blunting of velocity profiles across the channel increases. In the absence of significant particle migration the velocity profile indicates the presence of slip between the fluid and particle velocities near the wall of the channel. The magnitude of fluid velocity fluctuations measured from PIV analysis show increasing behavior with the shear rate. As the particle concentration increases, the fluid velocity fluctuations in both flow and spanwise direction increase. Close to the wall appreciable shear gradient exist and the free-surface undergoes fluttering motion due to convecting and rotating particles. Analysis of the spectra of the refracted light from the free-surface shows that flow structures of many length scales are present. These results are in qualitative agreement with the earlier findings of Loimer et al. (2002) and Timberlake and Morris (2005). Supporting the findings of Loimer et al. we have observed that as the particle fraction increases the autocorrelation in flow direction declines faster until a critical fraction is reached, thereafter the autocorrelation function decays slowly. We have studied the free-surface roughness and associated flow structure in velocity–velocity gradient plane. We observed formation of structured vortices at the free-surface which convect with the mean flow. We believe that the fluctuation in the normal stresses coupled with the flow structures at the free-surface induce the surface roughness. The results from our channel flow experiments are different from the observation of Timberlake and Morris (2005) in their experiments on falling film of suspension. This is due to the migration of the particles towards the free-surface in the falling film experiments which is absent in our studies. Also, the stereoscopic PIV study of Timberlake and Morris could not capture these free-surface patterns. These structural vortices, observed in our study, are expected to strongly affect the dynamics at the free-surface thus controlling the roughness patterns. However to quantify the height of the roughness pattern it is desired to study the motion in velocity–vorticity plane. Measurement of normal stresses at the interface will give valuable information to estimate the stress field needed to develop the correct model for the shear induced migration in film flow.

References

Adrian, R.J., Keane, R.D., Zhang, Y., 1995. Super resolution particle-imaging velocimetry. Meas. Sci. Tech. 6, 754–768.
Brady, J.F., Carpen, I.C., 2002. Second normal stress jump instability in non-Newtonian fluids. J. non-Newt. Fluid Mech. 102, 219–232.
Christensen, K.T., Soloff, S.M., Adrian, R.J., 2000. Technical Report 943, Department of Theoretical and Applied Mechanics, University of Illinois at Urbana-Champaign.
Govindarajan, R., Nott, P.R., Ramaswamy, S., 2001. Theory of suspension segregation in partially filled horizontally rotating cylinder. Phys. Fluids 13, 3517–3520.
Jenkins, J.T., McTigue, D.M., 1990. Transport processes in concentrated suspensions: the role of particle fluctuations. In: Joseph, D.D., Schaffer, D.G. (Eds.), Two Phase Flow and Waves. Springer-Verlag, New York.
Jin, Bo, Acrivos, A., 2004. Theory of particle segregation in rimming flow of suspensions containing neutrally buoyant particles. Phys. Fluids 16 (3), 641–651.
Karnis, A., Goldsmith, H.L., Mason, S.G., 1966. The kinetics of flowing dispersions: concentrated suspensions of rigid particles. J. Colloid Interface Sci. 22, 531.
Koh, C.J., Philip, H., Leal, L.G., 1994. An experimental investigation of concentrated suspension flows in a rectangular channel. J. Fluid Mech. 266, 1–32.
Kumar, S., Gupta, R., Banerjee, S., 1998. An experimental investigation of the characteristics of free-surface turbulence in channel flow. Phys. Fluids 10, 437–456.

Leighton, D., Acrivos, A., 1987. The shear-induced migration of particles in concentrated suspensions. J. Fluid Mech. 181, 415–439.

Loimer, T., Nir, A., Semiat, R., 2002. Shear-induced corrugation of free interfaces in concentrated suspensions. J. Non-Newt. Fluid Mech. 102, 115–134.

Morris, J.F., Bouley, F., 1999. Curvelinear flow of non-colloidal suspensions: The role of normal stresses. J. Rheol. 43, 1213.

Nott, P.R., Brady, J.F., 1994. Pressure driven flow of suspensions: simulation and theory. J. Fluid Mech. 275, 157–199.

Phillips, R.J., Armstrong, R.C., Brown, R.A., Graham, A.L., Abott, J.R., 1992. A constitutive equation for concentrated suspensions that accounts for shear-induced particle migration. Phys. Fluids A (4), 30–40.

Rashidi, M., Hetsroni, G., Banerjee, S., 1992. Wave-turbulence interaction in free-surface channel flows. Phys. Fluids A (4), 2727–2738.

Shauley, A., Averbakh, A., Nir, A., Semiat, R., 1997. Slow viscous flows of highly concentrated suspensions. Int. J. Mult. Flow 23, 613–629.

Singh, A., Nott, P.R., 2000. Normal stresses and Microstructure in bounded sheared suspensions via Stokesian dynamics simulations. J. Fluid Mech. 412, 279–301.

Singh, A., Nott, P.R., 2003. Experimental measurements of normal stresses in sheared Stokesian suspensions. J. Fluid Mech. 490, 293–320.

Sinton, S.W., Chow, A.W., 1991. NMR flow imaging of fluids and solid suspensions in Poiseulle flow. J. Rheol. 35, 735.

Timberlake, B.D., Morris, J.F., 2002. Concentration band dynamics in free-surface Couette flow of a suspensions. Phys. Fluids 14, 1580–1589.

Timberlake, B.D., Morris, J.F., 2005. Particle migration and free-surface topography in inclined plane flow of a suspension. J. Fluid Mech. 538, 309–341.

Tirumkudulu, M., Mileo, A., Acrivos, A., 2000. Particle segregation in mono-dispersed sheared suspensions in a partially filled rotating horizontal cylinder. Phys. Fluids 12, 1615–1618.

Zarraga, I.E., Hill, D.A., Leighton, D.T., 2000. The characterization of the total stress of concentrated suspensions of noncolloidal spheres in Newtonian fluids. J. Rheol. 44, 185–220.